J. Fluid Mech. (2009), *vol.* 634, *pp.* 91–111. © 2009 Cambridge University Press
doi:10.1017/S0022112009007502 Printed in the United Kingdom

Long's vortex revisited

RICHARD E. HEWITT† AND PETER W. DUCK

School of Mathematics, The University of Manchester,
Oxford Road, Manchester M13 9PL, UK

(Received 24 November 2008 and in revised form 13 March 2009)

We reconsider exact solutions to the Navier–Stokes equations that describe a vortex in a viscous, incompressible fluid. This type of solution was first introduced by Long (*J. Atmos. Sci.*, vol. 15 (1), 1958, p. 108) and is parameterized by an inverse Reynolds number ϵ. Long's attention (and that of many subsequent investigators) was centred upon the 'quasi-cylindrical' (QC) case corresponding to $\epsilon = 0$. We show that the limit $\epsilon \to 0$ is not straightforward, and that it reveals other solutions to this fundamental exact reduction of the Navier–Stokes system (which are not of QC form). Through careful numerical investigation, supported by asymptotic descriptions, we identify new solutions and describe the full parameter space that is spanned by ϵ and the pressure at the vortex core. Some erroneous results that exist in the literature are corrected.

1. Introduction

The structure and development of vortices is of key interest in many areas of both technological and environmental flows. Central to this field of interest are the contributions made by Long (1958, 1961), which have since driven a large number of subsequent publications.

What Long (1958, 1961) achieved was the rational development of an ordinary differential system that describes an *exact* (vortex) similarity-type solution to the Navier–Stokes equations for a viscous incompressible unbounded fluid. The solutions are exact in the sense that no approximations are required to obtain them from the framework of the full Navier–Stokes system (all have conical self-similarity).

The system derived by Long (1958, 1961) was presented in terms of a cylindrical-polar coordinate system and is governed by two control parameters: the 'flow force' (a conserved integral quantity) and an inverse Reynolds number ϵ (we will provide the exact definitions of these quantities when formulating the problem in the next section). However, Long's attention was focused exclusively on the boundary layer (quasi-cylindrical (QC)) limit and did not consider the analogous finite-Reynolds-number flow. A careful solution of the resulting boundary value problem was provided by Long (1961) in this QC limit.

Because of the practical importance of these types of flow, a great many papers have subsequently built upon QC theory, with the emphasis placed mostly upon the spatial/temporal stability of such flows. Notable amongst later works are the papers of Burggraf & Foster (1977), which considers the spatial marching of the corresponding parabolic partial-differential system, Drazin, Banks & Zaturska (1995), which presents results for Long's equations at finite Reynolds number and addresses their (spatial) stability, and Shtern & Drazin (2000), which considers the linear stability of the closely

† Email address for correspondence: richard.e.hewitt@manchester.ac.uk

https://doi.org/10.1017/S0022112009007502 Published online by Cambridge University Press

related half-line vortex states (which are distinct from the type of flow considered in this paper). For a thorough review of the area of swirling flows, readers are directed towards the comprehensive articles of Serrin (1972), Shtern & Hussain (1999) and Pillow & Paull (1985).

There are a number of closely related problems and boundary conditions that appear in the literature associated with this conically self-similar form. Solutions are typically subdivided into laterally bounded or unbounded domains, and also into subclasses that are either singular at a point, or singular along a (half) line. In many cases the problem is described in spherical polar coordinates, for which impermeability and circulation conditions are applied on a bounding conical surface. Such problems are typically distinct from the original Long's formulation, and can possess a different structure through the elimination of the subtle algebraic behaviour present in the laterally unbounded cylindrical formulation.

In this work we wish to concentrate on the formulation most closely related to the original work of Long (1961), namely a class of conically self-similar vortex solutions (described relative to a *cylindrical polar* coordinate system) for an unbounded fluid, with a singularity only at the origin. In this regard our equations of motion are precisely those of Long (1958, 1961) with a finite Reynolds number. This same problem has been tackled before in Drazin *et al.* (1995); however, we will show results that differ from theirs in a number of respects, most notably with regards to how non-uniqueness of the solutions develops. It should be mentioned that the numerical computation of the governing system is still a challenging task (even on modern computer hardware), and has to be carried out with a great deal of care. Our numerical approach is different from that applied by Drazin *et al.*; these authors used a numerical shooting procedure, whereas we have chosen to implement a more robust (but computationally more demanding) boundary-value/finite-difference algorithm. We will present solutions that are new to the literature and justify our numerical results (which disagree with those of Drazin *et al.*) by providing a selection of asymptotic descriptions that cover a number of limiting cases. Comparisons between the asymptotic predictions and our numerical data will also be presented.

The format of the paper is as follows. In § 2 we formulate the finite Reynolds number problem in the notation of Long's original work, including the boundary conditions for an unbounded flow. In § 3 we present detailed numerical solutions for the problem, including identifying non-unique solutions and limit points in the two-dimensional parameter space. In § 4 we are able to confirm a number of characteristics observed in our numerical results through asymptotic descriptions of several limiting cases. Finally, § 6 provides some discussion and overview of our results in the broader context of the existing literature.

2. Formulation

Following Long's original formulation of the problem, we consider the axisymmetric motion of an incompressible fluid of density ρ and kinematic viscosity ν. The system is described with respect to a cylindrical-polar coordinate system (r, φ, z) centred at the vortex axis and we solve for the flow in terms of a Stokes stream function $\psi(r, z)$ and a circumferential velocity component $v(r, z)$; the three cylindrical velocity components are then (u, v, w), where $u = -\psi_z/r$ and $w = \psi_r/r$.

As Long (1958, 1961) showed, the introduction of a similarity variable $x = r/z$ leads to an exact reduction of the Navier–Stokes system. In terms of this new variable, the

https://doi.org/10.1017/S0022112009007502 Published online by Cambridge University Press

flow quantities can be written in the form:

$$\psi(r,z) = \nu z\hat{f}(x), \quad v(r,z) = \frac{\nu}{r}m(x), \tag{2.1a}$$

$$p(r,z) = -\rho\frac{\nu^2}{z^2}h(x), \tag{2.1b}$$

where $p(r,z)$ is the pressure. For this form of solution, the meridional flow velocities are

$$u(r,z) = -\frac{\nu\hat{f}(x)}{r} + \frac{\nu\hat{f}'(x)}{z}, \quad w(r,z) = \frac{\nu\hat{f}'(x)}{r}. \tag{2.1c}$$

There is a dimensionless parameter associated with this solution, which is effectively an inverse Reynolds number

$$\epsilon = \frac{\nu}{K}, \tag{2.1d}$$

where the constant K is the circulation at infinity, that is, $rv \to K$ as $r \to \infty$.

In the original formulation there is a second parameter associated with a conserved 'flow force' (M in Long's notation); however, in this work we will prefer to treat the pressure at the axis of the vortex as the second parameter instead (the appropriate M can then be computed from any state *a posteriori*). We will say more about this below when describing the boundary conditions.

Following Long's formulation further, we use the same boundary layer scalings (but we make no assumptions about the size of ϵ)

$$y = \frac{x}{\epsilon\sqrt{2}}, \quad f(y) = \hat{f}(x), \quad \Gamma(y) = m(x)\epsilon \quad \text{and} \quad s(y) = h(x)\epsilon^4, \tag{2.2}$$

which results in the final form of the governing equations:

$$\Gamma^2 + 2y^3s' = -\epsilon^2(f^2 - ff'y + y^2f'' + 8y^4s - yf' + 4y^5s') - \epsilon^4(2y^4f''), \tag{2.3a}$$

$$yf'' - f'(1-f) - 4y^3s = -\epsilon^2(2f''y^3), \tag{2.3b}$$

$$y\Gamma'' - \Gamma'(1-f) = -\epsilon^2(2\Gamma''y^3 + 4\Gamma'y^2). \tag{2.3c}$$

2.1. *Boundary conditions*

At the axis of the vortex we impose the boundary conditions

$$f(0) = \Gamma(0) = 0 \quad \text{and} \quad s(0) = p_0. \tag{2.4}$$

It is straightforward to show that in the near-axis region, these conditions lead to a local behaviour of the form

$$f(y) = \bar{a}_1y^2 + O(y^4), \tag{2.5a}$$

$$\Gamma(y) = \bar{b}_1y^2 + O(y^4), \tag{2.5b}$$

$$s(y) = p_0 + \bar{c}_1y^2 + O(y^4), \tag{2.5c}$$

and the flow is non-singular except at $r = z = 0$. In this expansion the higher order terms are determined as functions of the unknowns $\bar{a}_1$, $\bar{b}_1$ and $\bar{c}_1$.

As noted above, one may view the arbitrary axis pressure p_0 as replacing the 'flow force' constraint introduced by Long (1958, 1961). This formulation is numerically more convenient than specifying the integral constraint because it maintains the banded structure of the discretized boundary value problem. Once a solution has

https://doi.org/10.1017/S0022112009007502 Published online by Cambridge University Press

been determined in this way, we can then determine the flow force via

$$M = \pi \int_0^\infty [(f'(y))^2 - 4y^2 s(y)] y^{-1} \, \mathrm{d}y. \tag{2.6}$$

This quantity is obtained by integrating the axial momentum equation over a constant z plane; the reader is referred to Long's original discussion for further details.

The appropriate conditions in the far field are rather more subtle for general values of ϵ (than for $\epsilon = 0$). As $y \to \infty$, it is straightforward to observe that, in general,

$$f(y) = a_1 y + a_2 + \frac{a_3}{y} + O(y^{-2}), \tag{2.7a}$$

$$\Gamma(y) = 1 + \frac{b_1}{y} + O(y^{-2}), \tag{2.7b}$$

$$s(y) = \frac{c_1}{y^2} + \frac{c_2}{y^3} + O(y^{-4}). \tag{2.7c}$$

In the QC case of $\epsilon = 0$ (as considered by Long, 1958, 1961) one may easily conclude that $c_1 = 1/4$ and then $a_1 = a_2 = 1$ and $b_i = 0$ for all $i \geqslant 1$ (leading to exponential, rather than algebraic, decay of Γ to the far-field value of unity). However, for general Reynolds numbers $\epsilon > 0$ the coefficients a_i, b_i, c_i will have a functional dependence on ϵ and p_0 that cannot be known *a priori*, although we can determine that $a_1^2 = 4c_1$. To accommodate this general far-field behaviour in our numerical scheme, we will truncate the domain at some finite value $y = y_\infty$ and then impose the two constraints:

$$\Gamma(y_\infty) - 1 + \Gamma'(y_\infty) y_\infty = 0, \tag{2.8a}$$

$$[f'(y_\infty)]^2 - 4[y_\infty^3 s'(y_\infty) + 3y_\infty^2 s(y_\infty)] = 0. \tag{2.8b}$$

Substitution of (2.7) into (2.8) demonstrates that these conditions are $O(y_\infty^{-2})$ accurate.

The fifth-order system (2.3), subject to the five boundary conditions (2.4) and (2.8) then forms a well-posed problem with solutions existing in a two-dimensional parameter space spanned by ϵ and p_0. It is this parameter space that we now explore, with particular attention on taking the (high Reynolds number) limit of $\epsilon \to 0$, rather than following Long's approach of simply setting $\epsilon = 0$.

3. Numerical results

We begin by presenting numerical results for the solution of (2.3) subject to (2.4) and (2.8). The problem is formulated as five first-order equations for the unknowns f, f', Γ, Γ' and s, solved by second-order finite-differencing coupled with Newton iteration. The discrete equations are solved at the mid-points of a non-uniform (adaptive) nodal distribution $\{y_i\}$ where $0 \leqslant i \leqslant N-1$, for some integer N where $y_0 = 0$ and $y_{N-1} = y_\infty$. The two conditions (2.8) are imposed at the mid-point $1/2(y_{N-1} + y_{N-2})$ using an appropriate second-order difference approximation at that point. The resulting matrix problem is banded and solutions are continued by applying the arclength continuation method of Keller (1977) with a bordering algorithm used to include the additional arclength constraint whilst still maintaining the advantage of the (mostly) sparse matrix structure.

A wide range of values for y_∞ and N were employed in our numerical scheme. As we shall see, some of the solutions we find have growing length scales for which we have used values for y_∞ as high as 1.2×10^5, whereas some QC solutions can

https://doi.org/10.1017/S0022112009007502 Published online by Cambridge University Press

be captured with $y_\infty = 10^2$ or less. Similarly a range of uniform, non-uniform and self-adapted meshes have been used to ensure reliable results. Typical values for N can range from 10^3 to 1.5×10^5. At the larger values of y_∞ the mesh points were typically not uniformly distributed. All of the numerical results presented herein are independent (to within the accuracy presented) of the mesh $\{y_i\}$ and the far-field parameter y_∞.

3.1. *The QC results with* $\epsilon = 0$

To begin with we recompute the known states for the case $\epsilon = 0$, our motivation for doing so is to validate the numerical approach and to clarify the relationship between the parameterization in terms of M or p_0. Our results agree with those already in the literature and figure 1(a) shows the traditional view of the solutions, whilst the alternative parameterization in terms of p_0 is shown in figure 1(b) and, finally, the connection between the flow force M and the axis pressure p_0 is shown in figure 1(c). The two limiting branches along which $M \to \infty$ can be associated with the two limits $p_0 \to \infty$ and $p_0 \to 0^+$. We do not present any velocity/stream function profiles at this stage, as many can be found in the existing literature in this special case.

3.2. *The results at general values of* $\epsilon > 0$

Having reproduced the classical results we now move on to the general case of finite Reynolds number, $\epsilon > 0$. This case has been addressed previously in Drazin *et al.* (1995); however, we will show considerable disagreement between our numerical results and those presented in their work.

The general features of note for $\epsilon > 0$ are: (i) for small values of ϵ there is a critical axial pressure below which a solution cannot be located due to the presence of a limit point, (ii) a pair of alternative disconnected states are possible which are also connected by a limit point and (iii) additional limit points can be found at larger values of ϵ, leading to a complicated solution space.

In figure 2 we again present the QC results (as the solid line) of figure 1(b) (for $\epsilon = 0$) together with the four solutions that are available for $\epsilon = 0.1$. It is clear that one of the four solution branches (S_1) is a finite-Reynolds-number continuation of the QC state, but this can no longer be continued to small axial pressures because it develops a limit point b at a critical p_0. This limit point then reveals a second vortex state (branch S_2). For this value of ϵ there are two further new (isolated) solutions (again connected by a limit point a), which we shall refer to as solution branches S_3 and S_4. We note that only when $\epsilon = 0$ is $f'(\infty) = 1$ for all p_0, which is the horizontal solid line in figure 2(b).

In figure 3 we continue the loci of the limit points a and b, as shown in figure 2, in the parameter plane spanned by ϵ and p_0. We know from the results of figure 2 that, for small ϵ, the two limit points (a and b) are introduced at small values of p_0. The evolution of these two limit points, to larger values of p_0, as ϵ is increased is shown in figure 3; the asymptotic description of these points will be discussed below. At rather larger values of ϵ the solution structure becomes more complicated. At $\epsilon \approx 0.24$ and $p_0 \approx 0.041$ we find a transcritical bifurcation (denoted by T in figure 3). At $\epsilon \approx 0.25$ an additional limit point c arises, which is associated with solutions that can be continued to negative values of p_0, then at $\epsilon \approx 0.258$ and $p_0 \approx 0.038$ a hysteresis point (denoted by H in figure 3) is obtained.

The evolution of the solution structure for fixed values of the pressure p_0 and varying ϵ is provided in figure 4. In figure 4(a) the axis pressure constant is $p_0 = 0.045$, for which figure 3 shows there to be three limit points a, c and e. For this p_0 solution

https://doi.org/10.1017/S0022112009007502 Published online by Cambridge University Press

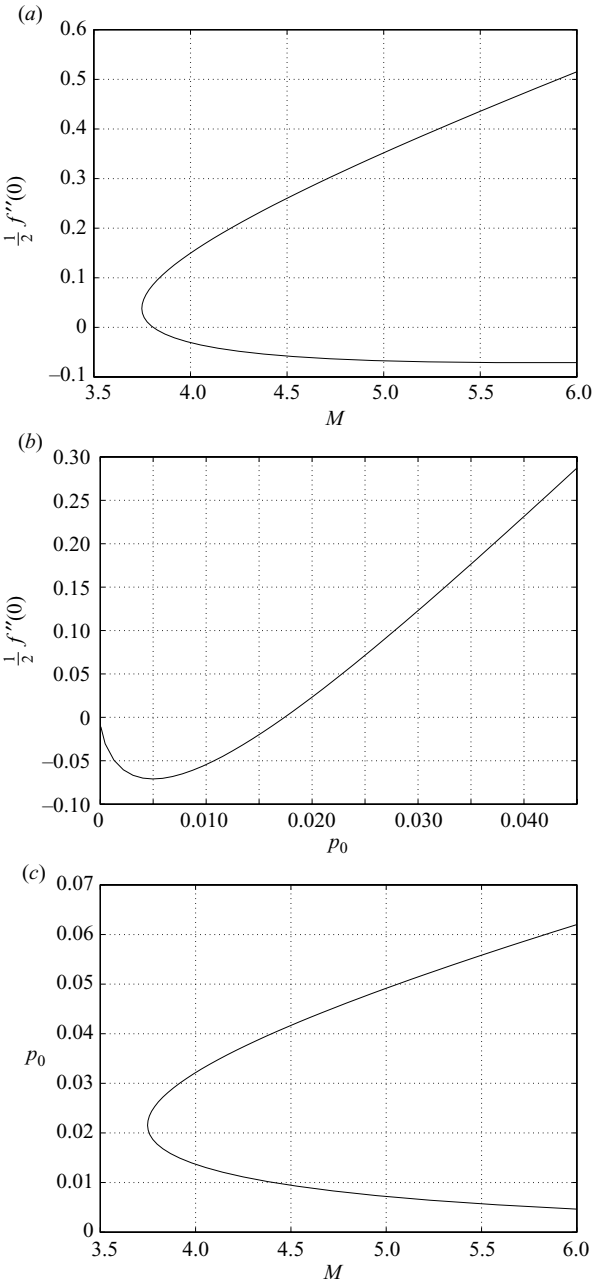


FIGURE 1. A reproduction of Long's original results for the QC equations ($\epsilon = 0$). In terms of the 'flow force' (M) there is a limit point at $M \approx 3.75$. However, when parameterized by the axis pressure (p_0) there is a single branch of solutions.

S_1 (which is connected to Long's original vortex state as $\epsilon \to 0$) has a small region of hysteretic behaviour on passing through limit points e and c and solution S_2 remains disconnected from it. For values of p_0 below the transcritical point T shown in figure 3, S_1 and S_2 reconnect, leading to the limit points b and d; this behaviour is shown in figure 4(b) at $p_0 = 0.039$. Finally, at values of p_0 below the point denoted by

https://doi.org/10.1017/S0022112009007502 Published online by Cambridge University Press

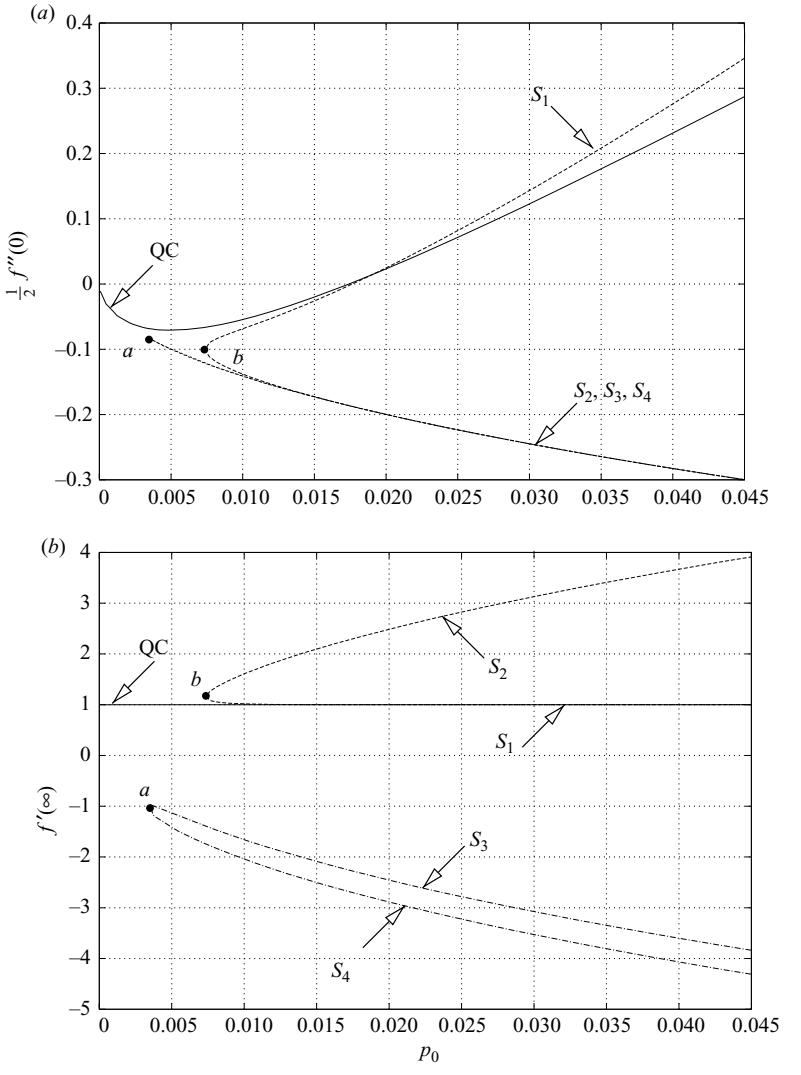


FIGURE 2. Solutions at fixed values of ϵ and varying axial pressure p_0. In figure (a) we show the reference solution of figure 1(b) for $\epsilon = 0$ (solid) together with the four solutions available for $\epsilon = 0.1$ (dash and dash-dot). Long's metric of $f''(0)/2$ does not distinguish the multiple solutions especially well, so in (b) we show an alternative measure $f'(\infty)$. Solid circles denote the presence of limit points, which arise at finite Reynolds number.

H in figure 3, the hysteretic behaviour at higher values of ϵ is removed as limit points d and e merge. The metric we use in figure 4 is the gradient of the circulation at the axis. Small values of this measure are associated with solutions that have a growing length scale (e.g. $S_{2,3,4}$ as $\epsilon \to 0$) whilst large values indicate a decreasing length scale.

In figure 5 we show sample profiles of the functions related to the axial flow, circulation and pressure in the similarity form of (2.1), namely, $f'(y)$, $\Gamma(y)$ and $s(y)$; the axial flow is proportional to $f'(y)/y$. In figure 5(a–c) we show profiles at the same values of $\epsilon = 0.1$, $p_0 = 0.04$, for each of the solutions S_1–S_4 shown in figure 2(b). We can clearly see that S_2 develops over a length scale that is an order of magnitude

https://doi.org/10.1017/S0022112009007502 Published online by Cambridge University Press

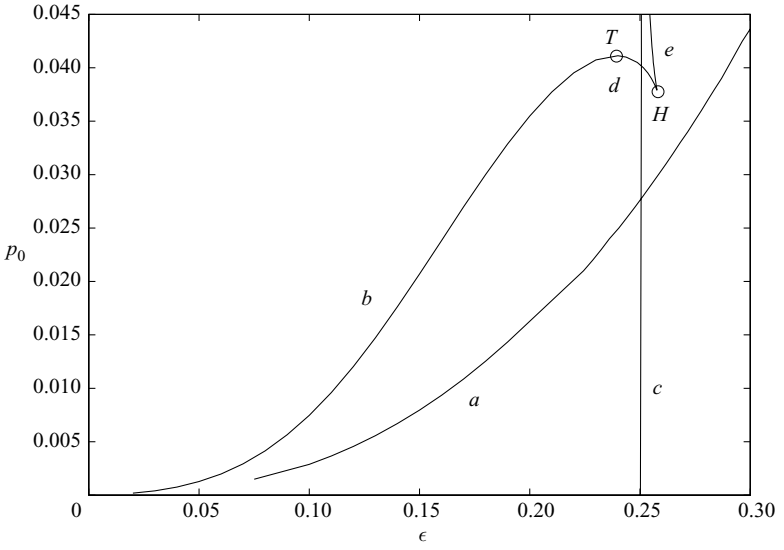


FIGURE 3. The loci of limit points in the parameter plane spanned by the inverse Reynolds number ϵ and the pressure at the axis p_0. The labelling of the lines is consistent with the labelling of the two limit points shown in figure 2. Further, the open circles H and T indicate a hysteresis point joined by d and e and a transcritical point joined by d and b, respectively. Both a and b approach the origin as $\epsilon \to 0$ (see later asymptotic descriptions); however, the computation involves increasing domain sizes that cannot be captured numerically.

larger than for the S_1 state, and contains a region of reverse axial flow where $f'(y) < 0$. Solutions S_3 and S_4 similarly develop over a length scale that is an order of magnitude larger than that found for S_2 and have $f'(y) < 0$ over their entire range (indicating that the axial flow is always towards the singularity, i.e. a sink-type flow). In figure 5(d) we show a case of $\epsilon = 0.3$, $p_0 = -0.1$. These solutions with negative pressure at the vortex axis (relative to the far field) only exist beyond the boundary, corresponding to the locus of limit point c in figure 3.

If we compare our results with those of Drazin *et al.* (1995) we find that there is little agreement for $\epsilon > 0$. Our system (2.3) is equivalent to (2.9)–(2.11) in their paper, although we retain the QC variables throughout in order to simplify the computations for small ϵ (see § 4 of Drazin *et al.* for the QC limit, for which their Reynolds number $R = 1/\epsilon$). None of the behaviour highlighted in figure 6 of Drazin *et al.* is obtained (for example the loop development at $R \approx 17$) and we believe their results are open to question. One possible source for this discrepancy is the boundary condition presented in Drazin *et al.* (e.g. (2.12), (5.2) and elsewhere in § 5 of their paper), which states that $F'(\infty) = 2^{-1/2}$ (equivalent to $f'(\infty) = 1$ in our notation). As we have noted above, this condition is only valid when $\epsilon = 0$. Our aim here is to support our own numerical results with some consistent asymptotic descriptions in § 4 below.

4. Limiting cases: support for the numerical results

4.1. $p_0 \to 0$ *in the infinite Reynolds number QC equations:* $\epsilon = 0$

We begin by considering the special case of the QC equations ($\epsilon = 0$) and addressing the limit of vanishing pressure at the vortex axis. If we denote the pressure at the axis

https://doi.org/10.1017/S0022112009007502 Published online by Cambridge University Press

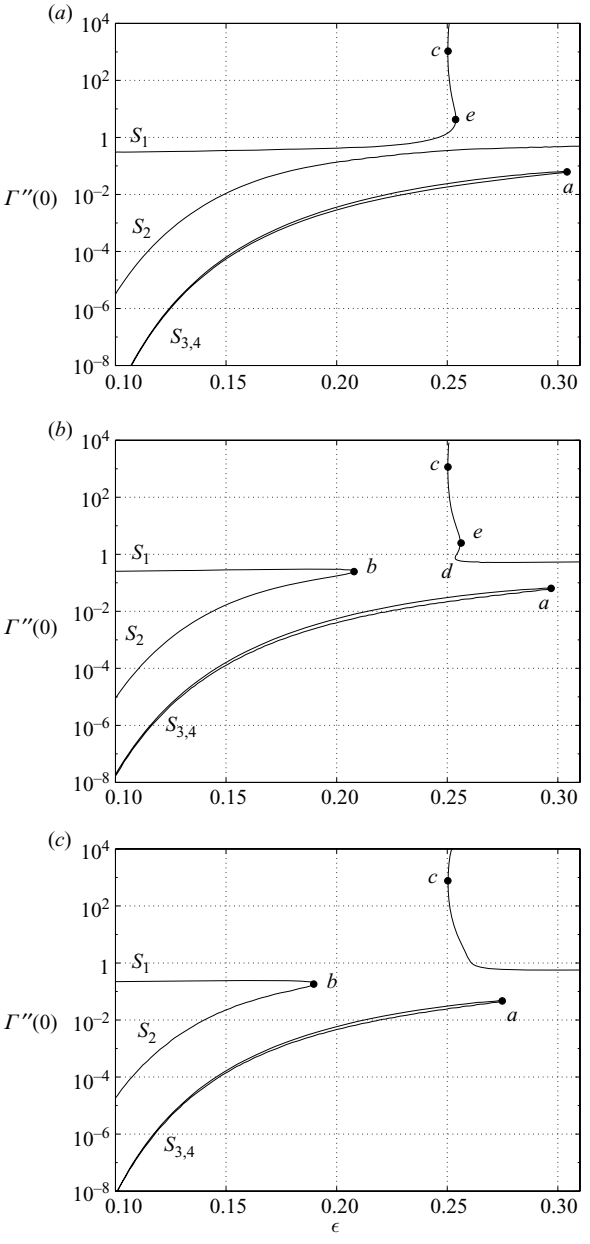


FIGURE 4. A view of the solution branches at constant values of p_0 chosen to be: (*a*) $p_0 = 0.045$, which is above the transcritical and hysterisis points denoted by (T) and (H) in figure 3, (*b*) $p_0 = 0.039$, which is between the hysteresis point (H) and the transcritical point (T) and (*c*) $p_0 = 0.035$, which is below both (H) and (T).

as $p_0 = \delta \ll 1$, then to describe the limit we introduce the expansions

$$s = \hat{s}_0(\hat{y})\delta + \cdots, \tag{4.1a}$$

$$f = \hat{f}_0(\hat{y})\delta^{-\frac{1}{2}} + \cdots, \tag{4.1b}$$

$$\Gamma = \hat{\Gamma}_0(\hat{y}) + \cdots, \tag{4.1c}$$

https://doi.org/10.1017/S0022112009007502 Published online by Cambridge University Press

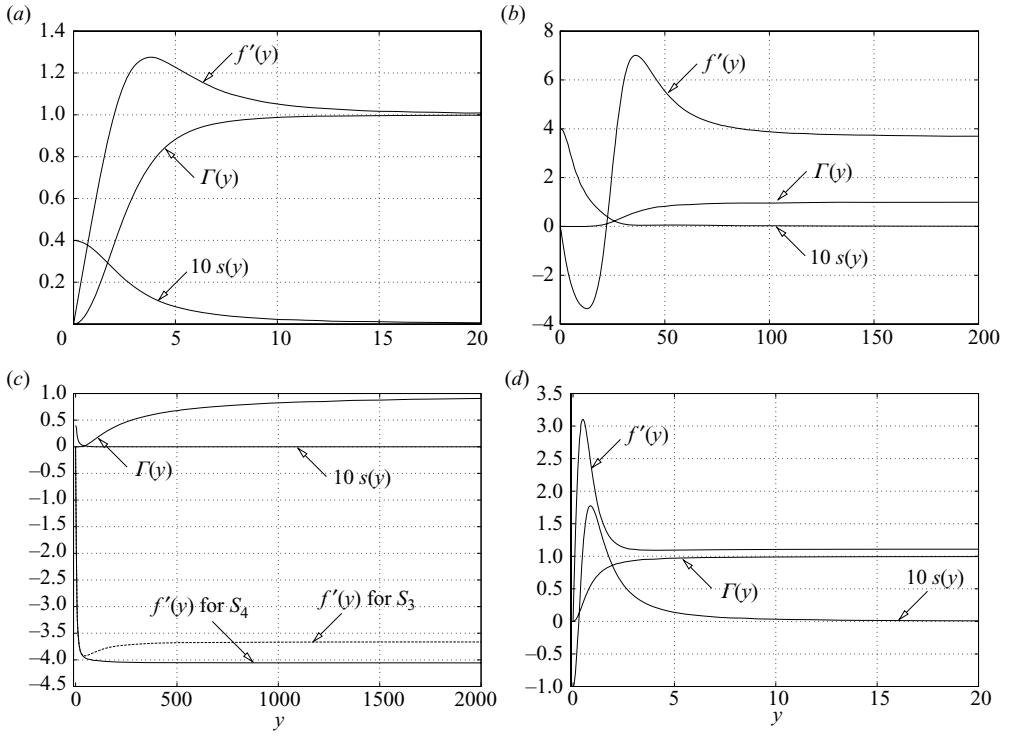


FIGURE 5. Profiles of the functions related to the axial flow, circulation and pressure ($f'(y)$, $\Gamma(y)$ and $s(y)$) for a range of solutions. (*a*) Solution S_1 at $\epsilon = 0.1$, $p_0 = 0.04$; (*b*) solution S_2 at $\epsilon = 0.1$, $p_0 = 0.04$; (*c*) solutions S_3 and S_4 at $\epsilon = 0.1$, $p_0 = 0.04$. In this case there is only a visible difference in the $f'(y)$ component for these two solutions, as we shall discuss in §4.4 below. (*d*) A solution with negative axial pressure (relative to the far field) at $\epsilon = 0.3$, $p_0 = -0.1$. Note that the coordinate scale for y differs from 20 to 2000 across the four figures.

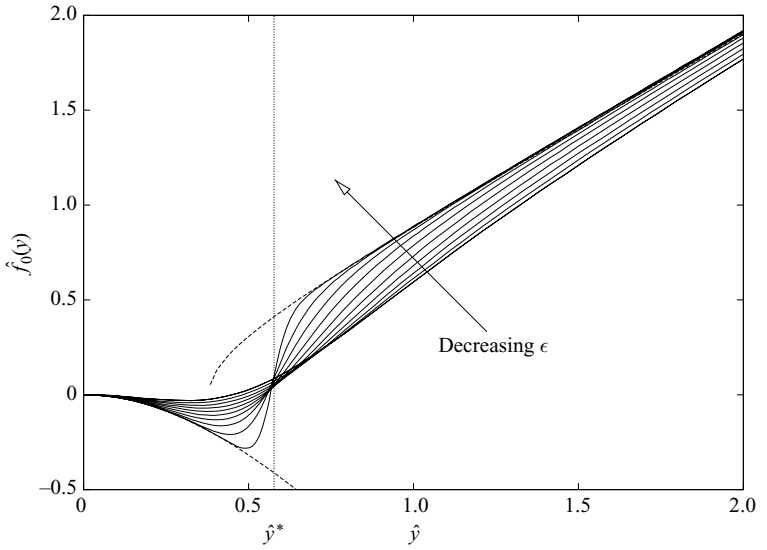


FIGURE 6. A comparison of the asymptotic prediction of (4.6) with numerical results as $p_0 \to 0$ with $\epsilon = \sqrt{p_0}$. The dashed lines are the leading-order asymptotic predictions in the two regions $\hat{y} > \hat{y}^*$ and $\hat{y} < \hat{y}^*$, whilst solid lines are the numerical results with $\epsilon = 0.1, 0.09, \ldots, 0.01$. The vertical line indicates $\hat{y}^*$, the predicted location of the displaced shear layer.

https://doi.org/10.1017/S0022112009007502 Published online by Cambridge University Press

where $\hat{y} = \delta^{1/2} y$. The leading-order equations are inviscid, namely

$$\hat{\Gamma}_0^2 + 2\hat{y}^3 \hat{s}_0' = 0, \tag{4.2a}$$

$$\hat{f}_0 \hat{f}_0' - 4\hat{y}^3 \hat{s}_0 = 0, \tag{4.2b}$$

$$\hat{\Gamma}_0' \hat{f}_0 = 0, \tag{4.2c}$$

subject to $\hat{f}_0(0) = \hat{\Gamma}_0(0) = 0$, $\hat{s}_0(0) = 1$ and $\hat{f}_0 \sim \hat{y}$, $\hat{\Gamma}_0 \to 1$, $\hat{s}_0 \sim 1/4\hat{y}^2$ as $\hat{y} \to \infty$. The leading-order solution in this case is easily obtained to be

$$\hat{\Gamma}_0 = \begin{cases} 0 & \hat{y} < \hat{y}^* \\ 1 & \hat{y} > \hat{y}^* \end{cases}, \quad \hat{s}_0 = \begin{cases} 1 & \hat{y} < \hat{y}^* \\ 1/4\hat{y}^2 & \hat{y} > \hat{y}^* \end{cases}, \tag{4.3a}$$

$$\hat{f}_0 = \begin{cases} \sqrt{2}\hat{y}^2 & \hat{y} < \hat{y}^* \\ \sqrt{\hat{y}^2 - 1/8} & \hat{y} > \hat{y}^* \end{cases}, \tag{4.3b}$$

where it can be shown that $\hat{y}^* = 1/2$ by requiring continuity of s_0 across $\hat{y} = \hat{y}^*$.

As we noted previously, the limit of $p_0 \to 0^+$ for this state corresponds to $M \to \infty$, where M is defined by (2.6). The large M limit has been considered previously by Foster & Jacqmin (1992), in which they derived the same leading-order description as presented above. Obviously we may also construct the appropriate viscous solution in a thin layer that spans the critical value of $\hat{y} = \hat{y}^*$, by introducing an additional coordinate $\eta = O(1)$ such that $y = \hat{y}^*/\delta^{1/2} + \eta$; the details of this are in Foster & Jacqmin (1992). We present the above result here because it leads directly to a finite-Reynolds-number analogue of this same structure.

4.2. $p_0 \to 0$ *for solution* S_1 *with large Reynolds number:* $\epsilon = O(\sqrt{p_0})$

If we now reconsider the same limit discussed in the previous subsection but for a finite Reynolds number, we know from the numerical results (see figure 2) that a limit point exists for S_1 at a critical p_0 when $\epsilon > 0$. To capture this behaviour we see that additional terms first appear (in particular in (4.2*a*)) when the relative size of the inverse Reynolds number is such that $\epsilon = k\delta^{1/2}$ for some constant k, where again $\delta = p_0$. In this case the scalings (4.1) are still appropriate, but now the leading-order system becomes modified by finite Reynolds number terms:

$$\hat{\Gamma}_0^2 + 2\hat{y}^3 \hat{s}_0' = -k^2 \left\{ \hat{f}_0^2 - \hat{y} \hat{f}_0 \hat{f}_0' + 8\hat{y}^4 \hat{s}_0 + 4\hat{y}^5 \hat{s}_0' \right\}, \tag{4.4a}$$

$$\hat{f}_0 \hat{f}_0' - 4\hat{y}^3 \hat{s}_0 = 0, \tag{4.4b}$$

$$\hat{\Gamma}_0' \hat{f}_0 = 0. \tag{4.4c}$$

Note that this system is still void of viscous terms and the first two equations are best re-posed in terms of a new quantity $\hat{h}_0 = -\hat{f}_0^2$, for which the governing equation is usefully linear:

$$(2\hat{y}^3 k^2 + \hat{y})\hat{h}_0'' - (4\hat{y}^2 k^2 + 3)\hat{h}_0' + 4\hat{y} k^2 \hat{h}_0 = 4\hat{y}\hat{\Gamma}_0^2. \tag{4.5}$$

Prompted by the form of the solution in the previous subsection, we solve (4.5) in two regions $\hat{y} < \hat{y}^*$ and $\hat{y} > \hat{y}^*$, with $\hat{\Gamma}_0$ as given in (4.3), although the location of $\hat{y}^*$ will in general differ. Because (4.5) is second order and we are solving in two regions, we have five unknown constants (the fifth being the value of $\hat{y}^*$). The corresponding five boundary conditions are $\hat{h}_0(0) = 0$ and $\hat{h}_0' \sim -8\hat{y}^3$ as $\hat{y} \to 0$, and near the critical value of $\hat{y}^*$ we require that both $\hat{h}_0$ and $\hat{h}_0'$ are continuous, whilst in the far field,

https://doi.org/10.1017/S0022112009007502 Published online by Cambridge University Press

$\hat{h}_0 \sim -\hat{y}^2$ as $\hat{y} \to \infty$. We now have a well-posed problem that determines the solution above and below $\hat{y}^*$ as well as the location of $\hat{y}^*$.

The solution for $\hat{h}_0$ is found to be

$$h_0(\hat{y}) = \begin{cases} -4(1 + k^2\hat{y}^2 - \sqrt{1 + 2k^2\hat{y}^2}) & \hat{y} < \hat{y}^* \\ A\sqrt{1 + 2k^2\hat{y}^2} - \hat{y}^2 & \hat{y} > \hat{y}^* \end{cases}, \tag{4.6a}$$

where

$$A = 4k^{-4} + (k^{-2} - 4k^{-4})\sqrt{\frac{4 + k^2}{4 - k^2}}, \tag{4.6b}$$

$$\hat{y}^* = \frac{1}{\sqrt{4 - k^2}}. \tag{4.6c}$$

It is clear from the form of (4.6) that a solution only exists for $0 \leqslant k < 2$, and we note that when $k = 0$ we recover the QC results of the preceding subsection. As $k \to 2$, we approach the limit point (denoted by '*b*' in figure 2) whilst additional terms must be reintroduced into the leading-order (shear layer type) system as $y \to y^*$.

In figure 6 we show a comparison of numerical results with the asymptotic predictions of (4.6) in the case of $\epsilon, p_0 \to 0$ with $\epsilon = p_0^{1/2}$; that is, $k = 1$. We note the excellent agreement between the limiting solution and the location of the shear layer at $y = y^*$. Similar agreement for the viscous shear layer solution can be generated, but we do not present the details here.

4.3. *The large-Reynolds-number limit $\epsilon \to 0$ with $p_0 = O(1)$ for solution branch S_2*

In this case the asymptotic description is rather more complicated than the previous limits. We begin by noting that there is no significant $O(1)$ region on the y scale and that, in the inviscid limit, these solutions develop on a $y_1 = \epsilon y$ scale as $\epsilon \to 0$. It is worth pointing out that this y_1 coordinate is comparable with the original (non-boundary layer) x coordinate introduced by Long (1958, 1961) (also see (2.2) above).

4.3.1. *Region I : $y_1 = \epsilon y$*

The appropriate expansions in this region are

$$f(y) = \frac{f_0(y_1)}{\epsilon^2} + f_1(y_1) + \cdots, \tag{4.7a}$$

$$\Gamma(y) = \gamma_0(y_1) + \gamma_1(y_1)\epsilon^2 + \cdots, \tag{4.7b}$$

$$s(y) = s_0(y_1) + s_1(y_1)\epsilon^2 + \cdots. \tag{4.7c}$$

The governing equations are then the analogue of (4.4) with $k = 1$ and we choose to drop the caret notation. The same approach can be taken here to develop a leading-order solution, which (subject to $f_0(0) = 0$, $s_0(0) = p_0$) is

$$f_0(y_1) = -2\sqrt{p_0(1 + y_1^2 - \sqrt{1 + 2y_1^2})}, \tag{4.8a}$$

$$s_0(y_1) = p_0\frac{\sqrt{1 + 2y_1^2} - 1}{y_1^2\sqrt{1 + 2y_1^2}}, \tag{4.8b}$$

$$\gamma_0(y_1) \equiv 0, \tag{4.8c}$$

after imposing the boundary conditions of $f_0(0) = \gamma_0(0) = 0$ and $s_0(0) = p_0$.

As $y_1 \to \infty$, $f_0 \sim -2\sqrt{p_0}y_1 + \sqrt{2p_0}$ and $s_0 \sim p_0/y_1^2$, and we consider the possibility of a further outer region on the $y = O(\epsilon^{-3})$ scale.

https://doi.org/10.1017/S0022112009007502 Published online by Cambridge University Press

4.3.2. *Region II* : $y_3 = \epsilon^3 y$

The appropriate expansions in this region are

$$f(y) = \frac{F_0(y_3)}{\epsilon^4} + \frac{F_1(y_3)}{\epsilon^2} + \cdots \,, \tag{4.9a}$$

$$\Gamma(y) = \Gamma_0(y_3) + \Gamma_1(y_3)\epsilon^2 + \cdots, \tag{4.9b}$$

$$s(y) = S_0(y_3)\epsilon^4 + S_1(y_3)\epsilon^6 + \cdots. \tag{4.9c}$$

The leading-order equations are then

$$F_0^2 + 8y_3^4 S_0 - y_3 F_0 F_0' + 4y_3^5 S_0' + 2y_3^4 F_0'' = 0, \tag{4.10a}$$

$$4y_3^3 S_0 - F_0 F_0' - 2y_3^3 F_0'' = 0, \tag{4.10b}$$

$$4y_3^2 \Gamma_0' + 2y_3^3 \Gamma_0'' + F_0 \Gamma_0' = 0, \tag{4.10c}$$

to be solved subject to matching constraints as $y_3 \to 0$ (i.e. (4.8) as $y_1 \to \infty$).

We begin by noting that there is a rather simple solution to this system:

$$F_0 = -2\sqrt{p_0} y_3, \tag{4.11a}$$

$$S_0 = p_0 / y_3^2, \tag{4.11b}$$

$$\Gamma_0 = \exp(-\sqrt{p_0}/y_3). \tag{4.11c}$$

This solution is simply the far-field solution of the y_1 system for f and s, but with a transition in the circulation. This straightforward solution is relevant to the other solution branches (S_3 and S_4, described below) but here we instead consider the possibility of an alternative solution to (4.10) that is not of the simple form of (4.11).

To solve for F_0 we can eliminate S_0 from the first two equations in (4.10), then divide by y_3^2 and integrate once to obtain

$$\frac{F_0^2}{y_3} - F_0 F_0' - 2y_3^3 F_0'' = 0, \tag{4.12}$$

where the constant of integration is found to be zero by considering the limit $y_3 \to 0$. On writing $F_0(y_3) = y_3 F(y_3)$ we can integrate the equation for $F(y_3)$ directly to yield that

$$F_0(y_3) = -2y_3\sqrt{p_0}\,\tanh\left(\frac{\sqrt{p_0}(1 - 4A_3 y_3)}{2y_3}\right), \tag{4.13a}$$

$$S_0(y_3) = \frac{p_0}{y_3^2}\,\tanh\left(\frac{\sqrt{p_0}(1 - 4A_3 y_3)}{2y_3}\right), \tag{4.13b}$$

where A_3 is a constant and then $\Gamma_0(y_3)$ can then be determined directly from the third equation of (4.10).

Note that (4.13*a*) and (4.13*b*) both satisfy the appropriate conditions as $y_3 \to 0$ (matching with the $y_1 \to \infty$ limit), whilst as $y_3 \to \infty$ we have

$$F_0(y_3) \sim 2y_3\sqrt{p_0}(1 - 2\exp(-4\sqrt{p_0}A_3)). \tag{4.14}$$

At this point, there is nothing to determine A_3 and our conjecture is that, because the asymptotic solution as $\epsilon \to 0$ solution develops exclusively in powers of ϵ^2 (as suggested by (2.3)), then we must have

$$A_3 = -\frac{\log \epsilon}{2\sqrt{p_0}}. \tag{4.15}$$

https://doi.org/10.1017/S0022112009007502 Published online by Cambridge University Press

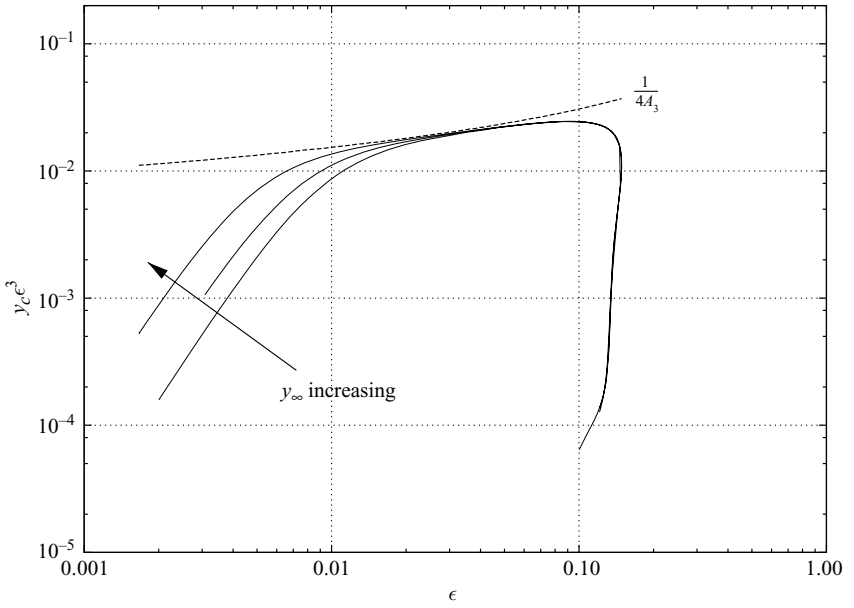


FIGURE 7. A comparison of the asymptotic prediction for the solution branch S_2 structure as $\epsilon \to 0$ (dashed) with the full numerical solution (solid) determined for $p_0 = 0.02$. Here we compute the value y_c where $f(y_c) = 0$ and compare it to the asymptotic prediction of $y_c = 1/(4\epsilon^3 A_3)$. To resolve the logarithmic region very large computational domains are needed; here we show $y_\infty = 10^4, 4 \times 10^4$ and 1.2×10^5.

We note that a logarithmic dependence of between A_3 and ϵ does not invalidate the expansions that gave rise to (4.13*a*).

To confirm our asymptotic prediction for the above asymptotic structure, in particular the quantity A_3, we begin computations on the S_1 branch at $\epsilon = 0.1$ and $p_0 = 0.02$ then arclength step, varying ϵ with p_0 fixed, to continue the solution around the limit point to branch S_2 and onwards towards $\epsilon = 0$. During this process, at each step we compute the critical value $y = y_c$ at which there is a zero streamline in the meridional flow, i.e. y_c is defined by $f(y_c) = 0$. According to the asymptotic description above, $y_c = 1/(4\epsilon^3 A_3) + \cdots$; in figure 7 we therefore compare $\epsilon^3 y_c$ with the asymptotic prediction of (4.15). Obviously, for any given choice of computational domain (i.e. choice of y_∞) there will be an ϵ that we cannot compute below because the length scales associated with the asymptotic structure of the vortex will be too large. It is for this reason that we can only show agreement for a range of ϵ. Even for computational domains of size 1.2×10^5, the critical value y_c will be at/beyond the edge of the computational domain for $\epsilon \leqslant 0.005$. Figure 7 illustrates an encouraging trend of our computed results towards our asymptotic result as ϵ decreases and y_∞ increases. Note that this asymptotic description also confirms the qualitative nature of the axial flow for this branch, which is directed towards the axis in the inner region, and away from the axis in the outer region (see figure 5*b*).

4.4. *The large-Reynolds-number limit $\epsilon \to 0$ with $p_0 = O(1)$ for solutions S_3 and S_4*

The asymptotic description of solution S_4 in the high-Reynolds-number limit is relatively simple. In this case the outer y_3 region plays only a minor role, whilst the y_1 layer is the dominant scale for all but the swirl component Γ. The solution is a

https://doi.org/10.1017/S0022112009007502 Published online by Cambridge University Press

repeat of that presented above in (4.7), (4.8) and the solution over the y_3 region is given by (4.11).

We now move on to the S_3 solution, which differs from the S_4 solution in that the y_3 region does play a slightly more important role, but only at higher orders in the expansion. On decreasing ϵ at fixed values of p_0, the S_3 and S_4 solutions become identical at leading order and only differ in higher order terms, which will vary over on the y_3 scale. An expansion to describe S_3 in the $y = O(\epsilon^{-3})$ region is then

$$f(y) = \frac{-2\sqrt{p_0}\, y_3}{\epsilon^4} + \frac{\tilde{f}(y_3)}{\epsilon^2} + \cdots, \tag{4.16a}$$

$$\Gamma(y) = \Gamma_0(y_3) + \tilde{\Gamma}(y_3)\epsilon^2 + \cdots, \tag{4.16b}$$

$$s(y) = \frac{p_0}{y_3^2}\epsilon^4 + \tilde{S}(y_3)\epsilon^6 + \cdots, \tag{4.16c}$$

where Γ_0 is as given in (4.11).

As before we can eliminate $\tilde{S}$ in the governing system, and divide by y_3^2. Integrating the resulting equation once we obtain a linearized form of (4.12), but this time with a non-zero constant of integration, which can be determined by matching to the $(\sqrt{2p_0})$ displacement produced by the inner y_1 region. We can repeat this process once more to obtain a first-order equation:

$$\frac{2\sqrt{2p_0}}{y_3}\left(\sqrt{p_0} - \frac{\tilde{f}}{\sqrt{2}}\right) + 2y_3\tilde{f}' - 2\tilde{f} = -2\sqrt{2p_0} - 2\sqrt{p_0}D_3, \tag{4.17}$$

where, again, the constant of integration is determined from matching to the inner region. In this expansion D_3 is a constant that can only be determined by matching this outer solution to the any linear growth of the correction term in the y_1 region as $y_1 \to \infty$. However, solving for the correction terms in the inner layer reveals that $f_1(y_1) \equiv 0$ and so $D_3 = 0$; the analysis is entirely straightforward and we do not present the details here.

The solution is therefore readily seen to be

$$\tilde{f}(y_3) = \sqrt{2p_0} + C_3\, y_3 \exp\left(-\frac{\sqrt{p_0}}{y_3}\right), \tag{4.18}$$

where C_3 is a constant that can only be determined from (yet) higher order terms in the expansion. The solution for $\tilde{S}$ then follows by back substitution into the governing system. When $C_3 = 0$ we have the simpler S_4 branch of solutions, and when $C_3 \neq 0$ we obtain the S_3 branch with a non-trivial y_3 layer. Note that both asymptotic descriptions confirm the qualitative feature of the axial flow, which is monotonic, directed towards the axis (see figure 5*c*).

To show that our numerical solutions are consistent with this asymptotic description it is not necessary to proceed to even higher (third) order in the expansion. Since (4.18) provides a prediction for the spatial form of the difference between S_3 and S_4 as $\epsilon \to 0$ we can compare it (without determining C_3) with our numerical results if we normalize the difference to be unity in the far field. To this end we may use (4.18) to predict that, as $\epsilon \to 0$,

$$\frac{\epsilon f'(y) + f_0'(\epsilon y)}{\epsilon f'(y_\infty) + 2\sqrt{p_0}} \sim \frac{\tilde{f}'(y_3)}{C_3} = \left(1 + \frac{\sqrt{p_0}}{y_3}\right)\exp\left(-\frac{\sqrt{p_0}}{y_3}\right), \tag{4.19}$$

https://doi.org/10.1017/S0022112009007502 Published online by Cambridge University Press

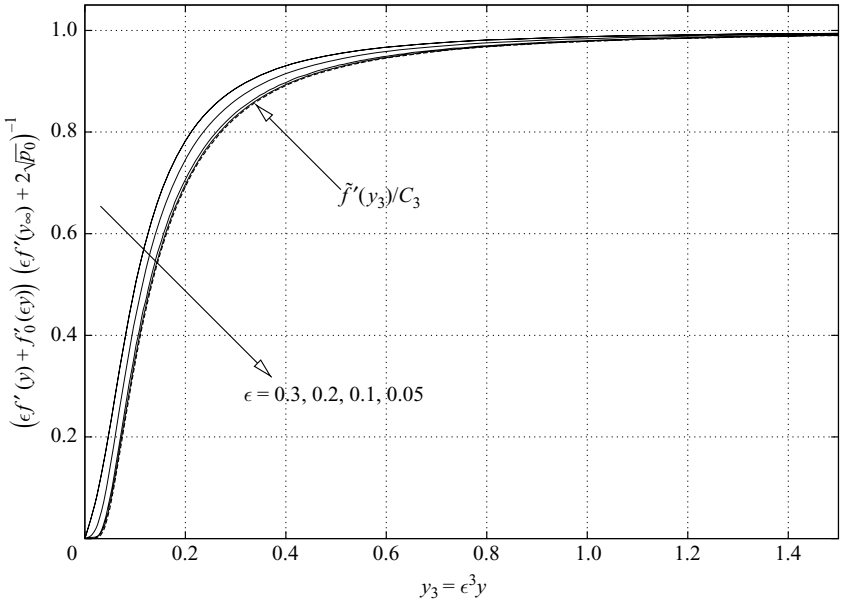


FIGURE 8. A comparison of the asymptotic description of (4.19) for solution S_3 with full numerical results in the high-Reynolds-number limit. The scaled numerical results are shown as solid lines and are presented for $p_0=0.05$ and $\epsilon=0.3, 0.2, 0.1, 0.05$; the asymptotic description as suggested by (4.19) is shown as the thicker dashed line.

where f_0 is given by (4.8). We present the comparison (4.19) in figure 8 and see that excellent agreement is found as $\epsilon\to 0$ for the solution branch S_3.

5. The physical features of the solution branches

Given the form of solution introduced in (2.1) we observe that the flow is only singular at the origin ($r=z=0$). In the meridional plane of the vortex, if we consider the limit of $r\to 0$ at fixed z, corresponding to $y\to 0$ with near-axis expansion (2.5), then the velocity components have the following form:

$$\frac{u}{\nu}\sim\frac{\bar{a}_1}{2\epsilon^2}\frac{r}{z^2}+\cdots, \tag{5.1a}$$

$$\frac{w}{\nu}\sim\frac{\bar{a}_1}{\epsilon^2}\frac{1}{z}+\cdots, \tag{5.1b}$$

$$\frac{v}{\nu}\sim\frac{\bar{b}_1}{2\epsilon^2}\frac{r}{z}+\cdots. \tag{5.1c}$$

Similarly, in the limit of $z\to 0$ at fixed r, the far-field expansion (2.7) leads to

$$\frac{u}{\nu}\sim-\frac{a_2}{r}+\cdots, \tag{5.2a}$$

$$\frac{w}{\nu}\sim\frac{a_1}{\epsilon\sqrt{2}}\frac{1}{r}+\cdots, \tag{5.2b}$$

$$\frac{v}{\nu}\sim\frac{1}{\epsilon}\frac{1}{r}+\cdots. \tag{5.2c}$$

https://doi.org/10.1017/S0022112009007502 Published online by Cambridge University Press

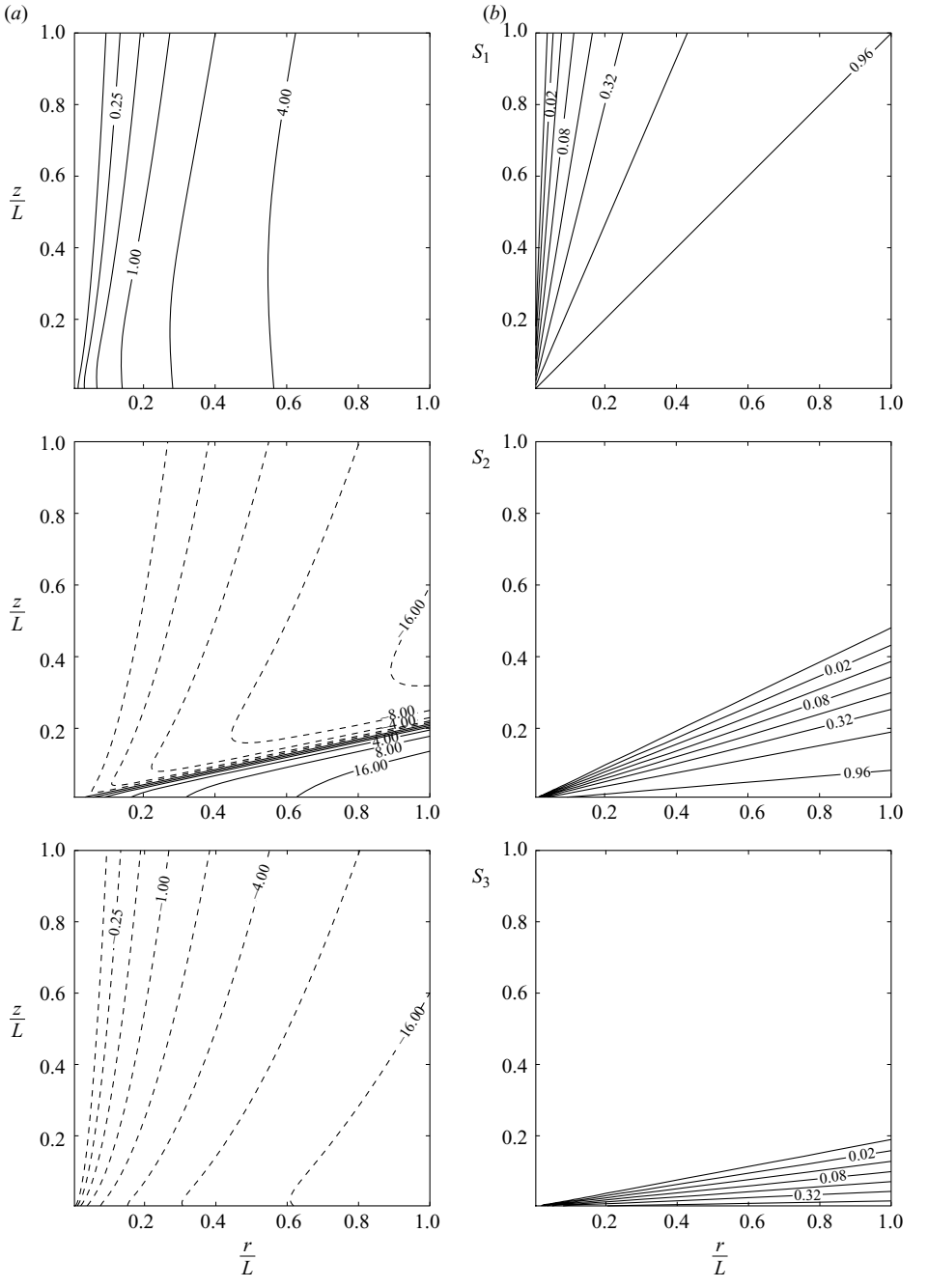


FIGURE 9. Contours of streamfunction $\psi/(\epsilon KL)$ (a) and contours of circulation rv/K (b) where L is an arbitrary length scale. All solutions are presented at the parameter values $p_0 = 0.04$ and $\epsilon = 0.1$. The solutions are (top to bottom) S_1, S_2 and S_3 (S_4 is not shown owing to its similarity to S_3). Dashed contours for the streamfunction indicate negative values.

In figure 9 we show the states presented in figure 5(a)–(c), but this time in the meridional r–z plane. For any arbitrary length scale L, we show contours of the non-dimensionalized streamfunction $\psi/(\epsilon KL)$ and the normalized circulation rv/K,

https://doi.org/10.1017/S0022112009007502 Published online by Cambridge University Press

where K is the far-field circulation of the vortex, as formulated in (2.1). Clearly the circulation has a simple conical self-similarity, and ranges from zero at the $r=0$ axis to unity in the 'far field'.

The solutions of figure 9 are shown at the parameter values $p_0=0.04$ and $\epsilon=0.1$, with streamlines shown on the left and contours of constant circulation shown on the right. The solutions are S_1, S_2 and S_3 (top to bottom) corresponding to figures 5(*a*)–(*c*), respectively. The solution S_1 is an outflow solution with mass transported in the direction of increasing z. The relatively small length scale of S_1 is highlighted by the near axis variation of the contours. It is this state which, if continued to high Reynolds numbers ($\epsilon \to 0$) would connect smoothly to the boundary layer vortex state described by Long (1958, 1961).

When varying the Reynolds number (i.e. varying ϵ) at fixed axis pressure, solution S_2 may arise either from S_1 through the limit point b shown in figure 4, or be an isolated state, depending upon the value of p_0. For $p_0=0.04$, figure 3 shows that S_1 and S_2 are connected by the limit point. The structure of S_2 is rather different from S_1, being a 'thicker' vortex state, as shown clearly by the shift in contours of constant circulation to larger radii. The thick reverse flow region near the axis corresponds to a potential flow (with zero circulation). The flow is towards the origin on $r=0$ and a zero streamline exists at a fixed angle to the axis of rotation. This S_2 state is qualitatively similar to that presented by Shtern & Hussain (1993), in which they associate the development of axial reverse flow and thickening of the vortex core to the phenomenon of vortex breakdown. Despite the superficial similarity there remain important differences between our S_2 state and that found by Shtern & Hussain. Chief amongst these differences is that the work of Shtern & Hussain imposes an impermeability condition along $z=0$ as well as a constant circulation (there is still slip along this boundary in their work). This is in stark contrast to the free nature of this boundary in the formulation of Long (1958, 1961) (and herein). In fact, in the limit of infinite Reynolds number the solution of Shtern & Hussain does not approach the Long solution (see their figure 19) as the 'outer' flow that exists between the vortex core and the bounding plane is non-trivial and contributes a finite flow force. Indeed, even the asymptotic description of the Shtern & Hussain solution differs in that they find a sudden transition in the circulation at a critical position, whereas we find an outer (thick) $O(\epsilon^{-3})$ transition region. Given the growing length scales (for $S_{2,3,4}$) as $\epsilon \to 0$ in the Long formulation, it is not surprising that distinct results are obtained when one imposes alternative 'far-field' boundary conditions.

The difference between solution branches S_3 and S_4 is slight, therefore in figure 9 we only show S_3. The much larger length scale over which the circulation varies for these solutions is clearly shown by the concentration of the circulation contours towards even larger radii. These states may be thought of as swirl affected sink/jet flows, with net transport of flow being towards the $z=0$ plane.

Intriguingly, although the problem as formulated here may be regarded as being forced by the circulation (at large distances from the axis), for the most part this plays only a minor role in the additional solutions we present. The new solutions can be shown to remain largely unaffected if the swirl (as $y \to \infty$) is omitted in the computations. This observation is reinforced by our asymptotic analyses, where generally the circulation does not affect the leading-order bulk flow. The main exception to this is in the vicinity of limit points (see, e.g. § 4.1). A corollary to this is that the other solutions may be regarded as extensions of jet flows that include the influence of circulation. Removal of the circulation leaves a class of jet flows that is

https://doi.org/10.1017/S0022112009007502 Published online by Cambridge University Press

obviously still exact within the context of the Navier–Stokes equations, and which, as far as the authors are aware, has not been described in the literature previously. In particular, it should be noted that this class of axisymmetric jet solution is distinct from the classical solutions, as catalogued in Rosenhead (1963). We must note that the limit of zero circulation is non-trivial for these solutions, in the sense that the dimension of the parameter space is reduced by one owing to the lack of a Reynolds number.

6. Discussion

In this paper we have presented a number of previously unreported solutions arising from the similarity reduction of Long (1958, 1961). This similarity form is an exact solution of the Navier–Stokes equations, based on the cylindrical-polar coordinate system with an isolated singularity at the origin. We can recover the well-known (QC) solution branch naturally in our numerical and asymptotic results (in the limit of vanishing inverse Reynolds number, $\epsilon \to 0$ and finite flow force M), but show that other limiting solutions are also possible.

The QC solution has received a great deal of attention in the past, in particular its stability characteristics have been extensively documented (Foster & Smith 1989; Foster & Jacqmin 1992; Shtern & Drazin 2000), much of the motivation arising from a desire to model geophysical problems including tornadoes (see, e.g. Burggraf & Foster 1977).

The additional solutions reported here indicate that three alternative solution branches can also exist as $\epsilon \to 0$ in addition to those arising directly from the classical solutions of Long (1958, 1961). Of most direct relevance to the solution of Long (which we have labelled S_1) is the alternative solution that we have labelled as S_2. The origin of this new solution can ultimately be traced to an inability to commute the limits of large flow force ($M \to \infty$) and large Reynolds number ($\epsilon \to 0$). In the formulation of Long, a boundary layer approximation is applied and finite Reynolds number effects are subsequently neglected; this approach yields solutions for which $p_0 \to 0^+$ (i.e. a diminishing pressure at the axis) as $M \to \infty$. However, we have shown that for any $\epsilon \ll 1$ there exists a critical $p_0 \sim \epsilon^2$ below which Long's states cannot be continued and instead join smoothly to the S_2 branch as the flow force is increased; for sufficiently small values of ϵ the S_2 branch is obtained as $M \to \infty$ in place of the Long's state that is typically described as 'type II' in the literature. However as ϵ is increased further, the solution space becomes increasingly complex, as we show in figure 3, and the limit point between S_1 and S_2 plays an important role in describing the system. Furthermore, from the physical point of view, at present there appears to be no reason why these additional states may not be relevant.

Our numerical results have been unable to confirm the previous work of Drazin *et al.* (1995), however it is worth emphasizing that many of the results presented here required lengthy computations on modern hardware (despite the system's appearance as a somewhat innocuous, albeit nonlinear, fifth-order ODE). To capture accurately the subtle far-field algebraic behaviour, disparate length scales and the additional solution branches require very large computational domains with large numbers of grid points. We treated the problem numerically as a boundary value problem rather than recasting it into an initial value problem (with an extra layer of iteration, as was the case in Drazin *et al.*). In figure 10 we show the same results as figures 5, 6 and 7 in Drazin *et al.*. In figure 10(*a*) there is clearly no evidence of the loop structure discussed in Drazin *et al.* that arises at $\epsilon \approx 1/17$ and $M \approx 5.3$. However, in

https://doi.org/10.1017/S0022112009007502 Published online by Cambridge University Press

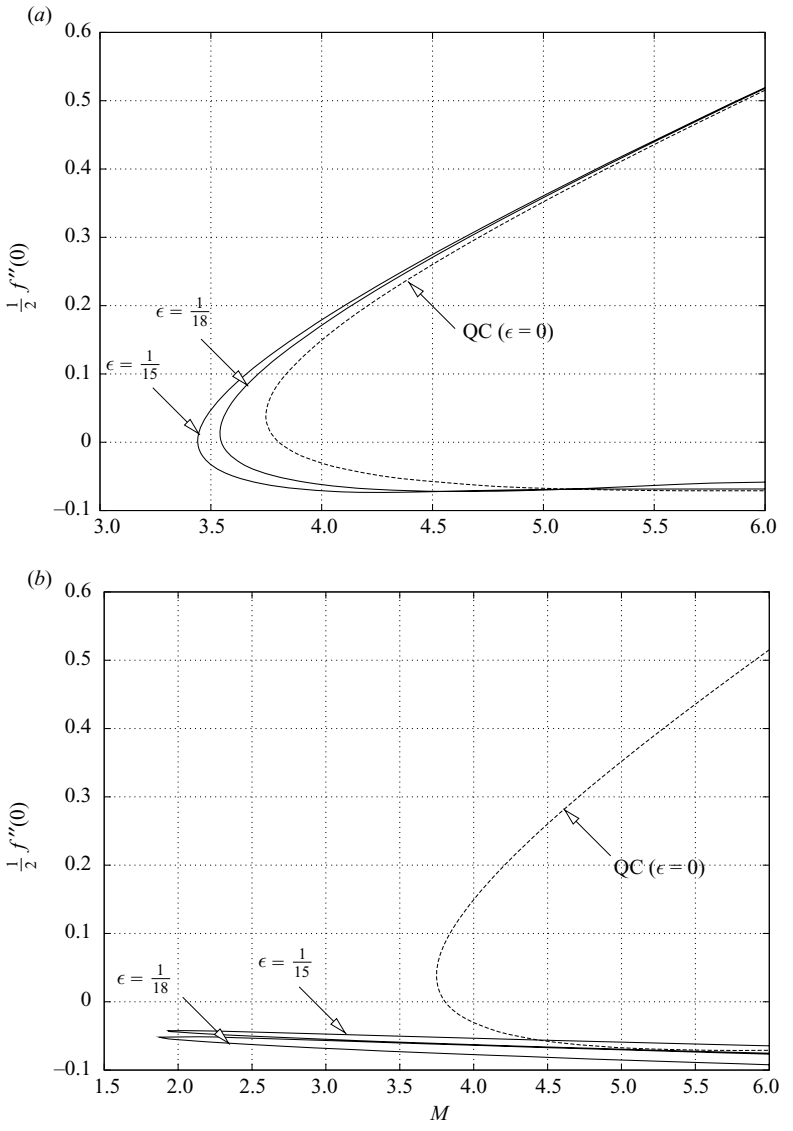


FIGURE 10. Solutions for comparison with those of Drazin *et al.* (1995) (in particular figure 6 of their paper). In (*a*) we show the standard QC results for varying flow force M together with the solutions $S_{1,2}$ at $\epsilon = 1/15,\ 1/18$. In contrast to Drazin *et al.*, we find no loop development on the lower branch at $\epsilon \approx 1/17$ and $M \approx 5.3$. In (*b*) we repeat the QC result again for reference, but this time include the additional solutions $S_{3,4}$ again for $\epsilon = 1/15,\ 1/18$.

figure 10(*b*) we do show the additional solutions of S_3 and S_4 and one may speculate that the proximity of these states may also cause some numerical difficulties for the initial value approach taken in Drazin *et al.*

Problems of this type (especially those linked to cylindrical or spherical polar geometries) are clearly of fundamental importance and still manage to reveal surprises as a result of continuing theoretical analysis and advances in computation. The question of the stability of these new states remains open.

https://doi.org/10.1017/S0022112009007502 Published online by Cambridge University Press

REFERENCES

Burggraf, O. & Foster, M. 1977 Continuation or breakdown in tornado-like vortices. *J. Fluid Mech.* **80** (04), 685–703.

Drazin, P., Banks, W. & Zaturska, M. 1995 The development of Long's vortex. *J. Fluid Mech.* **286**, 359–377.

Foster, M. & Jacqmin, D. 1992 Non-parallel effects in the instability of Long's vortex. *J. Fluid Mech.* **244**, 289–306.

Foster, M. & Smith, F. 1989 Stability of Long's vortex at large flow force. *J. Fluid Mech.* **206**, 405–432.

Keller, H. 1977 Numerical Solution of Bifurcation and Nonlinear Eigenvalue Problems (ed. P. H. Rabinowitz), pp. 359–384. Academic Press.

Long, R. 1958 Vortex motion in a viscous fluid. *J. Atmos. Sci.* **15** (1), 108–112.

Long, R. 1961 A vortex in an infinite viscous fluid. *J. Fluid Mech.* **11** (04), 611–624.

Pillow, A. & Paull, R. 1985 Conically similar viscous flows. Part 1. Basic conservation principles and characterization of axial causes in swirl-free flow. *J. Fluid Mech.* **155**, 327–341.

Rosenhead, L. 1963 *Laminar Boundary Layers*. Oxford University Press.

Serrin, J. 1972 The swirling vortex. *Phil. Trans. R. Soc. Lond.* A **271** (1214), 325–360.

Shtern, V. & Drazin, P. 2000 Instability of a free swirling jet driven by a half-line vortex. *Proc. R. Soc.* A **456** (1997), 1139–1161.

Shtern, V. & Hussain, F. (1993). Hysteresis in a swirling jet as a model tornado. *Phys. Fluids* **5**, 2183.

Shtern, V. & Hussain, F. 1999 Collapse, symmetry breaking, and hysteresis in swirling flows. *Annu. Rev. Fluid Mech.* **31** (1), 537–566.

https://doi.org/10.1017/S0022112009007502 Published online by Cambridge University Press